Investigation of structural and mechanical properties of BioCaCO3-LDPE composites

Serife Yalcin, Daniel Chateigner, Loïc Le Pluart, Stéphanie Gascoin, Sophie Eve

https://doi.org/10.33263/Materials12.029043

ISSN: 2668-5728 https://materials.international

Materials International

Volume 1, Issue 2, Pages 0029-0043
2019

Received: 26.11.2019
Accepted: 22.12.2019
Published: 30.12.2019

Article

Investigation of structural and mechanical properties of BioCaCO$_3$-LDPE composites

Serife Yalcın [1]*, Daniel Chateigner [2], Loïc Le Pluart [3], Stéphanie Gascoin [2], Sophie Eve [2]

[1] Harran University, Faculty of Arts and Science, Department of Physics, Osmanbey Campus, 63300, Sanliurfa, Turkey
[2] Normandie Université, Ecole Nationale Supérieure d'Ingénieurs de Caen (ENSICAEN), Université de Caen Normandie (UNICAEN), Centre National de la Recherche Scientifique (CNRS), Institut Universitaire de Technologie (IUT)- Caen, Laboratoire de CRIstallographie et Sciences des MATériaux (CRISMAT), 6, Bd M. Juin, 14050, Caen, France
[3] Normandie Université, ENSICAEN, UNICAEN, CNRS, Centre National de Recherche Technologique (CNRT), Laboratoire de Chimie Moléculaire et Thio-organique (LCMT), 6, Bd du Maréchal Juin 14050, Caen Cedex, France
* Correspondence: serifeyalcin@harran.edu.tr; Scopus ID: 17347094700

Abstract: The three different Mollusk shells, *Pecten maximus, Crepidula fornicata and Crassostrea gigas,* were studied and compared with synthetic and commercial powders. All samples were analysed by X-ray diffraction, Quantitative phase analysis, and quantitative line broadening (microstructure) analysis using the Combined Analysis method. LDPE-CaCO3 composites were prepared in a twin screw extruder in the composition range of 0–10.8 filler content. Ultimate Mechanical properties of dog-bone type injection molded tensile specimens (ISO-527-2-5A) were measured. Results are showing that the biogenic calcium carbonate is less efficient in improving polyethylene stiffness than the synthetic ones, independently of its crystalline form, to use stearic acid coating allows an improvement of the matrix stiffening. The yield strength is unchanged whatever the kind of filler used, which makes shell spares valid for reuse in polymer industry.

Keywords: Mollusk Shell, Combined Analysis, $CaCO_3$ filler, Coating, Mechanical properties.

1. Introduction

Mollusk shells that have been subject of numerous studies are high performance organic/inorganic enhancing bio-composite materials [1-3]. They exhibit excellent mechanical properties, thanks to their large resilience to crack propagation [4]. Since mineral calcium carbonate is hard and brittle and organic layers are soft materials [4], their combination inspired the development of high performance ceramic composites with an improved resistance to crack propagation [5-6]. Some researches have expressed that biogenic crystals have structural differences from from their fully mineral counterparts that potentially has important influence on some properties of [7-9].

Cite This Article: Yalcin, S.; Chateigner, D.; Le Pluart, L.; Gascoin, S.; Eve, S. Investigation of structural and meahnical properties of BioCaCO$_3$-LDPE composites. Mat Int **2019**, 1, 0029-0043.
https://doi.org/10.33263/Materials12.029043

Mollusk shells are composite biomaterials composed of 95 to 99 wt% of calcium carbonate, the remaining components forming the organic matrix [10-11]. They represent nowadays large amounts of spare sea shells discarded to the environment, after harvest and marketing, from aquaculture, farming, fishing, food, pearl, and canning industries [12-13]. These solid wastes, always associated to some organics, can participate to water and even decompose in the marine environment [14]. Consequently a reuse of shell spares would advantageously contribute to environmental issues. For instance, dispersion of nanofillers in a polymer matrix is assisted by strong interactions, enabling the preparation of polymer nanocomposites with higher loading of nanofillers [15].

Lazzeri et al. (2005) reported that an addition of precipitated calcium carbonate (average particle size 70 nm) to HDPE rises both Young modulus and yield stress, and decreases the impact strength, but that a stearic acid compatibilization treatment negatively affects these, compared to uncoated composites [16]. However, Gai et al. (2005) reported that the PP mechanical properties using powder fillers (average particle size 5.2 μm) are larger than those of PP materials produced using the original untreated powders [17]. On another hand González et al. (2006) incorporated sea shell wastes in various proportions (average particle size 78 μm) to PP and HDPE matrices and did not notice significant modification of the overall mechanical and rheological properties, except for an increase of the Young's Modulus [18]. A good agreement in montmorillonite/ polymer nanocomposites is shown between experimental measurements and predictions of tensile strength [19].

The purpose of this study is to examine the influence of ground biogenic sea shells addition to low density polyethylene (LDPE) on the mechanical properties and matrix crystallinity, by comparison with composites containing synthetic calcite and aragonite $CaCO_3$ particles. Ground shells are from three different mollusk species from Gastropoda and Bivalvia to test different $CaCO_3$ microstructures from broadly expended taxa. Powders are controlled with particle sizes under 1 μm to increase the specific filler/polymer interface in the composite.

2. Materials and Methods

2.1. Materials

Low density Polyethylene Flexirene MR50 (Polimeri Europa) and commercially available Calcium Chloride dehydrate, Potassium Hydrogen Carbonate and Calcium Carbonate (Sigma Aldrich, 10 μm mean particle size) were used. The filler particles are obtained by grinding non-biogenic powders, and biogenic mollusk sea shells from three different species: i) the gastropod *Crepidula fornicata,* the most abundant parasite along the ocean French coasts made of aragonitic $CaCO_3$ layers; ii) the edible bivalves *Pecten maximus,* the largest scallop made of calcitic layers and; iii) *Crassostrea gigas*, the most expanded oyster species over the world also made of calcitic layers. All samples were picked from dead animals on the Channel sea coast, Sword beach (49°17'52" N, 0°17'58" W). Stearic acid (Fluka AG) was used to avoid agglomeration during the grinding stage and potentially improve the dispersion state of calcium carbonate particles in the polymer matrix.

2.2. Fillers elaboration

Biogenic $CaCO_3$ fillers were obtained by powderising mollusk shells. Complete shells were introduced for grinding in laboratory with Retsch planetary ball milling machine (Retsch, Haan, Germany). The resulting powders are then composed of an average of the microstructures (aragonitic crossed lamellaes, foliated calcite, columnar, lath-type and rod type fibrous prismatic, chalky lenses, lamellar, parallel lamellar) composing the whole shell. To grind samples, we used different milling conditions because of the varying hardness between samples and to obtain the same mean particle sizes (as controlled using different grinding times and conditions). We ground each shell different grinding rotation speed and time because thickness and hardness of shells is different. The eventually remaining inside soft tissues were removed carefully and washed with pure water.

Purely mineral $CaCO_3$ fillers had also to go through some grinding in order to obtain similar grain sizes as in the case of biogenic grains. In this case we used a mixture of 10g of calcium carbonate, 50 ml of distilled water and 2 wt% of polyacrylic acid in the ball milling machine. The wet mixture obtained after two days of grinding at 300 rpm, 5 repetitions, 38 minutes, and then 300 rpm, 15 repetitions, 38 minutes, was dried at 80°C for one day in air.

The metastable synthetic aragonite calcium carbonate polymorph was prepared by precipitation according to the method of Lucas et al (2000) [20], at a temperature of 80°C to help aragonite formation [21]:

$$2\,KHCO_3 + CaCl_2 \rightarrow CaCO_3 + CO_2 + 2\,KCl + H_2O \quad (1)$$

After cooling down to room temperature, aragonite precipitates were washed with distilled water, and dried for one day at 120 °C.

Stearic acid fillers coating was obtained in the following way. After dissolution of 0,4 g of NaOH in 200 ml of distilled water, 1g of stearic acid was added under magnetic stirring at 250 rpm during 1h 45 min at a temperature of 80 °C. Then, 10 g of $CaCO_3$ was added to the solution for 2h. After filtration, the powder was washed with hot water to eliminate remaining pure stearic acid, before drying at 120°C for one day.

2.3. Composites elaboration

Whatever the powders (biogenic or not, coated or not, calcite or aragonite) used to elaborate the composites, Ground Calcium Carbonate (GCC) powders and low density Polyethylene (LDPE) were dried under vacuum conditions for a minimum of 24h before processing. Processing experiments are performed with a 15 cm^3 DSM Xplore (Geleen, Netherlands) corotating twin screw μ-extruder. The barrel temperature is set at 200ºC and the screw speed at 100 rpm. LDPE is melt blended with 10 of GCC during 2 min. Then, the blend is injected and molded with an Xplore 10 cm^3 injection unit in a mold whose temperature is set at 30ºC to obtain normalized tensile testing dog bone samples (ISO-527-2-5A) [22-23].

2.4. Samples Characterization

Sample's morphology and particle sizes were examined by Scanning Electron Microscopy (SEM, Carl ZEISS SUPRA 55) in secondary electrons mode. We used an applied voltage of 3kV, a 30 μm diaphragm aperture and a working distance of 4-10 mm, to avoid samples' charging as much as possible. Observations were performed on non-coated samples when this was possible. However, peculiarly for GCC-PE composites in which PE prevents any reasonable electrical conduction, carbon-sputtered sample surfaces were studied. We examined shell microstructures using fractured shell cross sections. The terminology of shell microstructures is usually based on the morphology of sub-units visible with a SEM. Shell microstructures were described using the terminology of Carter and Clark (1985), but emphasise that these definitions only represent a terminology (the names are convenient, brief summaries of observed morphologies), not necessarily a statement of homology. The`first-order' and `second-order' (prisms, lamellae), was used to describe increasingly fine microstructural elements with morphological distinction [24]. For instance, simple crossed lamellar structure is composed of `first-order lamellae' (approx. 10 μm thick), each of which is composed of `second-order lamellae' (1 μm in thickness). The shell reference frame is defined by the growth (**G**), margin (**M**) and normal (**N**) directions. More details of macroscopic shell frames and microstructural types can be found elsewhere [25].

All samples were analysed by X-ray diffraction using a D8 Advance Vario1 Bruker diffractometer equipped with a front Johansson Ge(111) monochromator and a LynxEye™ detector (using a detection window of 3°). We used the Cu $K\alpha_1$ radiation (λ = 1.54060 Å). The patterns were measured at room temperature in a 2θ range from 10° to 110° (0.0105° increment). The instrument aberrations were calibrated using the LaB_6 srmb standard from NIST. Quantitative phase analysis, quantitative line broadening (microstructure) analysis and unit-cell parameters were refined using the Combined Analysis method [26], using an enhanced Rietveld-like fit [27] with

the help of the MAUD (Materials Analysis Using Diffraction) software [28]. No attempt was made to refine atomic positions during the fits in our case of ground shells and powders, such parameters being best approached on textured layers [29]. Aragonite and Calcite initial structures used in the fits were taken from the Crystallography Open Database [30], entries n° 2100187 and 4502441 [31-32], with the respective space groups and unit-cell parameters (Pmcn: a=4.96Å, b=7.97Å, c=5.74Å and R-3c:H: a=4.99Å, c=17.05Å). When possible the mean crystallite shapes were refined within Combined Analysis using the Popa model [33].

Thermogravimetric analyses (TGA) were performed using a Perkin Elmer TGA 7 analyzer with a heating rate of 20°C.min^{-1} from 50 to 900 °C under nitrogen flow (80 ml/min). The value of the residue at 550°C (i.e. before $CaCO_3$ decarbonation) was used in order to determine the mineral content of the processed composite materials.

Crystallinity of the composites has been studied with Differential Scanning Calorimetry (DSC) using a Perkin Elmer DSC 4000 analyser, calibrated with indium, with a heating rate of 10°C.min^{-1} from 20 to 250 °C under nitrogen flow.

3. Results and Discussion

3.1. Microstructure and structure analyses using SEM and XRD

3.1.1. Biogenic $CaCO_3$

A cross sectional view of a *Pecten maximus* flat valve (Figure 1a), taken at 2/3 of the shell radius (far from the myostracum) illustrates the complex architecture of the Shell. From the Inner (bottom) to the Outer (top) sides of the valve, a stacking of all calcitic Complex Crossed Lamellar (ICoCL), Intermediate Irregular Prisms (IIP), and Complex Crossed Lamellar (CoCL) layers are observed, with varying thicknesses along the growth direction (horizontal). The ICoCL layers are made of bladelike lamellaes, typically 10 micrometers long, 1 µm wide and 0.1 µm thick (Figure 1b), with their largest surface approximately parallel to the (**G**,**M**) plane. The lamellaes group into bundles of several hundreds which intersect each others at angles of around 120° (Figure 1c) . The number of IIP layers varies from place to place in the shell with a general trend to lower or even disappear close to the juvenile growth stage. Also, at some places and more often at adult stage, some lamellae intercalate between some irregular prism layers (Figure 1a, between the two top most IIP layers, zoomed in Figure 1d). The prisms are indeed very irregular in shape (Figure 1e), neither made of subunits as in columnar nacre of *Turbo undulatus* [26] nor forming well delineated paralepiped as in calcite prisms of *Atrina serrata* [35]. Except just below the adductor muscle, a location which we tried to remove as much as possible for our analyses, the mineral part of all the shell layers is calcite (Supplementary material Figure S1), with a refined value of 99.8(3)%. The refined cell parameters of this calcite are a=4.99(5)Å and c=17.08(2)Å, representing 0.03% and 0.16% of relative cell distortion along the two main axes respectively. Such weak levels of cell distortions are commonly observed in biogenic calcite layers [32] when the layers are powderized. The mean coherent size domains after grinding are refined as roughly equisized (56(3) nm) prisms, i.e. the individual first-order lamellae of the ICoCL and OCoCL have been reduced to few crystallites along their thickness and typically 10 along their widths.

Crepidula fornicata cross sections reveal three different layers, all of the crossed lamellar microstructure (Figure 2a). The Outer and Inner Comarginal Crossed Lamellar layers (OCCL and ICCL resp.) sandwich an Intermediate Radial one (IRCL). All first-order and second-order lamellaes (Figure 2b) for these three layers are of similar shapes and sizes as those observed in other gastropods like *Charonia lampas* [29], with several micrometers long laths and typically submicronic sizes in the other two directions. As usual in Crossed Lamellar layers, the major mineral part is aragonite, with only 1.7(3)% of calcite (Supplementary material Figure S2). The refined unit-cell parameters of aragonite are a=4.96 (2)Å, b= 7.96 (4)Å and c= 5.75(3)Å, *i.e.* no cell distortion along a, and only 0.05% distortions along b and c axes compared to non biogenic

aragonite. Since all crossed lamellar layers do not exhibit the same level of cell distortions [2], we observe here the average distortion coming from all three layers cumulated to the powderizing effect, both tending to distortions isotropization. The mean crystallites after grinding are revealed elongated along their c-axes (70.6(6) nm) and quasi isotropic along the other two main directions (32.4(9) nm and 31.0(9) nm along **a** and **b** axes resp.). As previously for the calcite layers of *Pecten maximus*, several crystallites are necessary to build up the elongated laths seen in SEM images, but a full Combined Analysis including a quantitative description of the layers' textures are required to give more reliable descriptions [29].

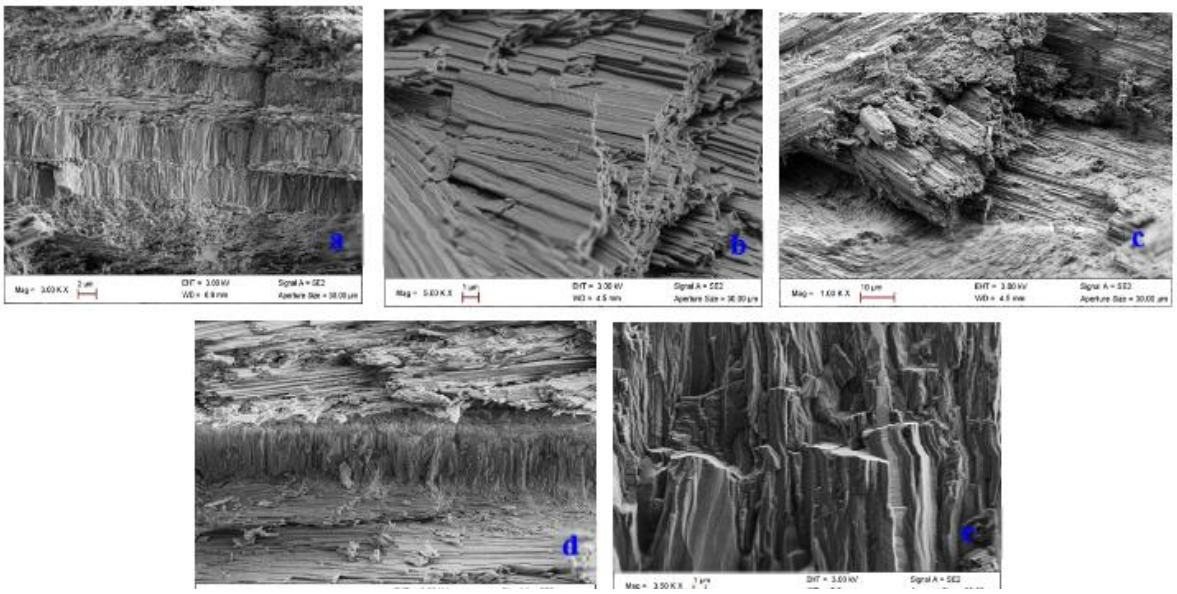

Figure 1. SEM observation of a cross section of the flat valve of *Pecten maximus*. a) global view at approximately 2/3rd of the total shell along **G**. b) zoom on first-order lamellaes of the OCoCL top layer. c) Intersected bundles of first-order lamellaes. d) One IIP layer sandwiched between the ICoCL and OCoCL layers at 1/5th of the total shell. e) zoom on the irregular prisms of the IIP layer.

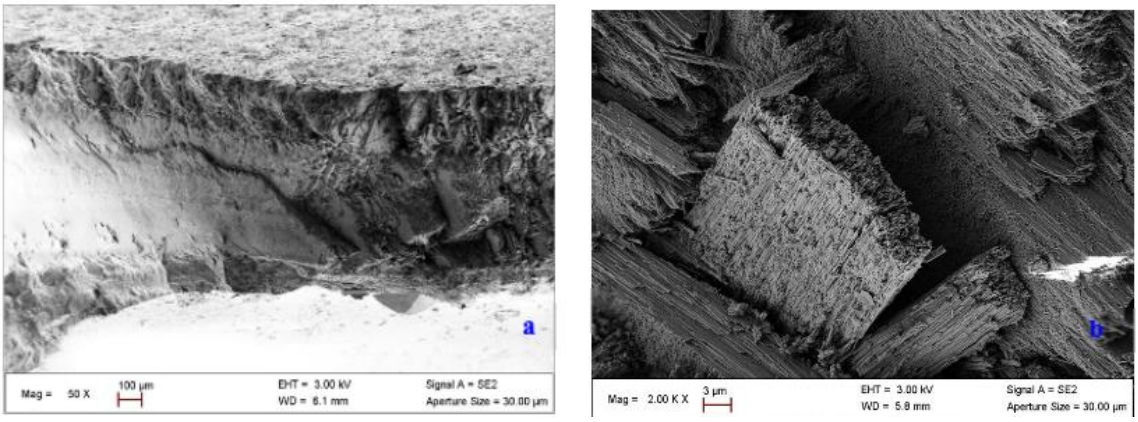

Figure 2. SEM observation of a cross section of the *Crepidula fornicata* shell. a) global view at approximately 2/3rd of the total shell along **G** (Outer an Inner sides of the shell are at top and bottom resp. **G** is horizontal, **N** vertical. b) zoom on first- and second-order lamellaes of the ICCL layer.

The second, fully calcitic bivalve *Crassostrea gigas* which we undertook in this study (Figure 3), is made of several microstructural layers, mainly foliated calcites (FC) located in the inner parts of the Shell, and an Outer Prismatic Calcite (OPC). This complex stacking incorporates at least four different types of microstructures including chalky-like [35], prisms [36], granular and semi-nacres [37], all containing only calcite as mineral (Supplementary material Figure S3). With refined

cell parameters of a=4.99(1)Å and c=17.05(6)Å, the 0.03% and 0.01% relative distortions are again very small, and probably averages of more pronounced ones existing in the original biogenic textured layers. Indeed, strong textures have been observed in *Crassostrea gigas* layers [38 and 39], without analysed consequences on cell distortions. The mean crystal sizes after grinding are also roughly isotropic (58(2) nm and 52(3) nm along **c** and **a** axes resp.), and much smaller than the grain sizes visible in SEM images. Only the platelets (Figure 3c) of semi nacre might be made of a single crystallite along their thickness.

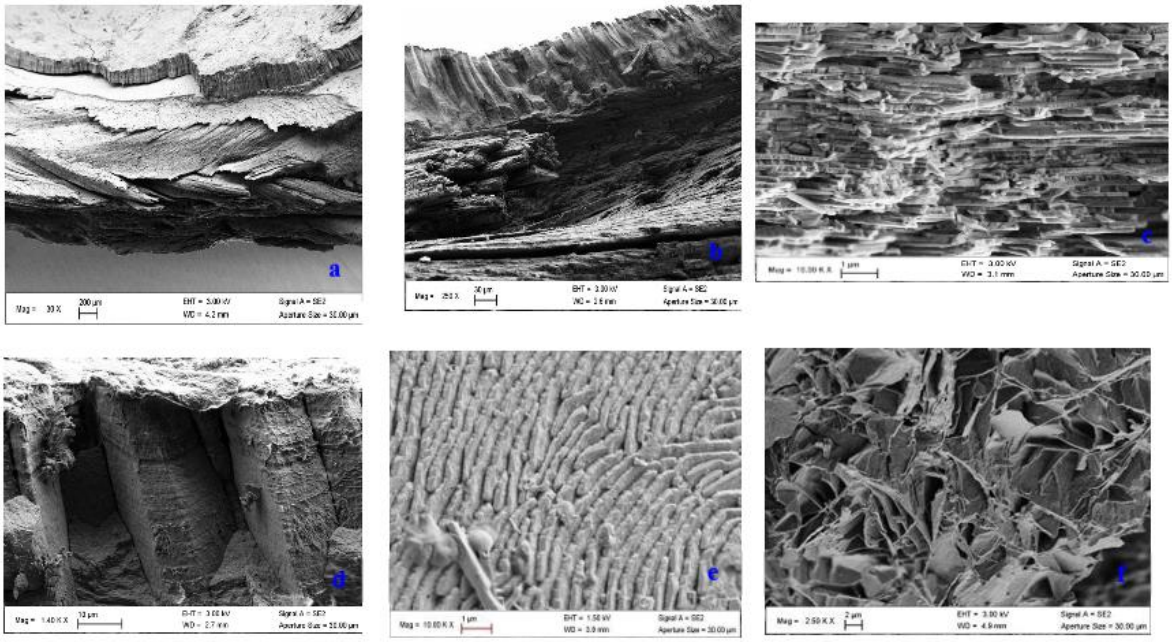

Figure 3. SEM observation of a cross section of the flat valve of *Crassostrea gigas* shell. **a)** Complex architecture made of several microstructural layers, foliated and prismatic calcites. **b)** outermost layers (Outside is at top, **G** is horizontal, **N** vertical), showing a foliated calcite layer and the outer prisms. **c)** zoom on semi nacre tablets, **d)** outer prisms, **e)** Foliated calcite and **f)** chalky calcite.

The three selected shell species represent large variations in microstructural types, *i.e.* distant organic matrices, including two different calcium carbonate polymorphs (aragonite and calcite) exhibiting very different elastic behaviours, and for the calcite polymorph different microstructural elements (prisms, tablets, laths). Biogenic calcite and aragonite might offer different bondings to the polymer matrix via their organic elements, and together with their mineral constituants result in different plastic and elastic characteristics of the $CaCO_3$-PE composites [40].

3.1.2. Non-biogenic $CaCO_3$

3.1.3. Ground and Stearic Acid coated samples

Sample grinding can affect not only crystal and grain sizes, but also introduce microstrains and cell distortions. In the case of commercial calcite, our grinding conditions revealed a crystallite mean size reduction (Supplementary Figure S4c and d) by typically 15 times after grinding (150(2) nm). On the other hand, the microstrain level and cell distortion are insignificantly modified (3.7(4) 10^{-4} r.m.s., a = 4.99(6) Å and c = 17.06(3) Å respectively). The mean crystallite shapes are also modified under grinding (Supplementary Figure S4 b and c insets), from roughly spherical in the as received calcite powder to more rhomb-like in the ground sample. Such shape modification associated to the crystallite size decrease indicates that some gliding system has been activated during grinding, linked to the rhombohedral planes of calcite. Consequently, the only effect that grinding operates on calcite crystals is to decrease their mean sizes via crystalline gliding activation, hereby increasing the coating specific surface, without any significant increase in internal energy via defect creation and cell distortions. The aspect of calcite

after grinding can be seen on Supplementary Figure S5b.

A very similar process occurs while grinding shell layers (Supplementary Figure S1, 2 and 3), although initial crystals formed various and different habits. Ground biogenic calcite layers (Supplementary Figure S1 and 3) also exhibit rhomb-like calcite crystals, *i.e.* inter- and intra-crystalline molecules do not hinder intrinsic mineral deformation processes in such layers. In these shell powders we recognize initial microstructural elements present in the shells, *e.g.* lamellae of *C. fornicata* (Supplementary Figure S2 inset) and *Pecten maximus* (Supplementary Figure S1 inset) or foliae of *C. gigas* (Supplementary Figure S3 inset), together with more roundish and smaller grains due to grinding indicating that this latter did not affect all initial crystals.

Ground calcium carbonate particles usually exhibit strong tendency to aggregate, which would prevent good dispersion within the final composite. Therefore, a suitable surfactant for the surface treatment of these particles is necessary, to hinder aggregates formation. As in previous works we chose Stearic Acid (SA) to ensure full coverage of the particles, whether biogenic or not [41-42]. Once SA coated, ground calcite indeed appears more homogeneously distributed, with a lower level of aggregation than the uncoated calcite (Supplementary Figure S6).

Synthesized aragonite and commercial calcite powders exhibit needle-like (Supplementary Figure S4a) and rhombic (Supplementary Figure S5a) grains respectively. Such crystal shapes are usual for these two polytypes of calcium carbonate. Aragonite exhibits average grain lengths and widths varying in the 10-55 µm and 0.5-3.5 µm ranges respectively. The mean crystallite sizes of calcite as determined from XRD (Supplementary Figure S4c) is 2400(200) nm with a low level of microstrains (3.4(1) 10^{-4} r.m.s.) and cell parameter distortions (a = 4.99(4) Å and c = 17.06(2) Å).

3.2. Composite materials

3.2.1. SEM characterisation of filler dispersion in composite materials

The dispersion and spatial distribution of fillers in the composites were investigated by SEM on plastically fractured composites samples after tensile testing. From Figure 4, it can be concluded that the composites processing does not significantly decresase nor increase the calcite aggregates size since the particles observable are similar in size and aspect to those of the Supplementary Figures S5 and 6. On the other hand aragonite needles seem to have been fractured during the processing since their average length is strongly reduced. Moreover it appears clearly that the interfacial interactions between uncoated particles and the polyethylene matrix are weak. No embedded particles are detectable suggesting the failure if the composites originated from their interface with the matrix during polyethylene plastic deformation. Because of lack of chemical bonding between matrix–filler and high stress in front of agglomerated particles, cracks propagate easily [43]. No polymer residue can be evidenced at the surface of these particles either. Therefore it can be concluded that the adherence level of the matrix to these uncoated synthetic particles is very low. Regarding biogenic fillers, the analysis on SEM pictures is more difficult due to the heterogeneous shapes of the $CaCO_3$ crystals. Biogenic calcite from oyster shells seem to show very low compatibility with the apolar polyethylene matrix since no residue is observed on aggregates present in the fractured region and that some decohesion zones are visible on partially embedded particles. Concerning biogenic aragonite, the adhesion level seems slightly higher since *C. Fornicata* particles remained embedded with polyethylene residue at their surface.

Figure 5 illustrates the influence of the stearic acid coating in the case of *Crepidula fornicata* in the polyethylene matrix, which is representative of all the characterised composites. The compatibility of the fillers with the apolar matrix has been improved since the $CaCO_3$ particles remain embedded in the matrix.

3.2.2. Composite properties

The mechanical properties of filled polymers depend on the filler mechanical properties and the quality of their interface with the polymer matrix, but they are also strongly related to the crystallinity of the matrix and to the filler content [44]. Table 1 reports the crystallinity values obtained from DSC

measurements, the filler content deduced from TGA analysis as well as the stiffness of the filled polymers (G* modulus obtained from DMA in torsion) and their ultimate tensile properties determined by tensile testing.

All the filled materials contain approximately 10 wt% of filler as initially planned except PE-*C. Gigas*, PE-*C. Fornicata* and PE-Calcite–SA which are significanlty less filled. This has been taken into account to evaluate the matrix crystallinity. The matrix crystallinity is slightly lowered for all the filled systems except those containing synthetic aragonite. For the biogenic $CaCO_3$ containing composites, no direct link between the $CaCO_3$ nature and the crystallinity of the matrix can be established. The SA coating does not seem to influence significantly the matrix crystallinity either. These slight changes in polyethylene crystallinity do not overcome the effect of filler incorporation on the polymer mechanical properties. Due to their intrinsic stiffness most fillers contribute to an improvement of the polymer matrix G* modulus. According to the data reported in Table 1, it seems that biogenic calcium carbonate is less efficient in improving polyethylene stiffness than the synthetic ones, independently of its crystalline form. This might be attributed to the greater tendency to form aggregates of the grinded mollusk shells and their lesser morphological homogeneity. Using stearic acid coating allows an improvement of the matrix stiffening, probabling by avoiding excessive aggregation and allows reaching modulus values which are of the same order as those obtained with synthtic calcite or aragonite. Regarding the yield strength, it is unchanged whatever the kind of filler used, which suggests that interfacial interactions are rather poor in those composites. This is confirmed by the strain at break values which are always lower than for pure polyethylene. This embrittlement is probably caused by earlier crack propagation initiated at the filler/polymer interfaces due to stress concentration and poor interfacial bonding.

The bonding to the polymer matrix which could have been expected with these various biogenic $CaCO_3$ forms due to the organic elements they contain is not significantly different from one species to another from a mechanical point of view. However these biogenic fillers are not detrimental to the polymers mechanical properties and allow reaching the same properties than traditionnally filled polymers. This opens the possibility to use these marine industrial wastes in the polymer compounding industry.

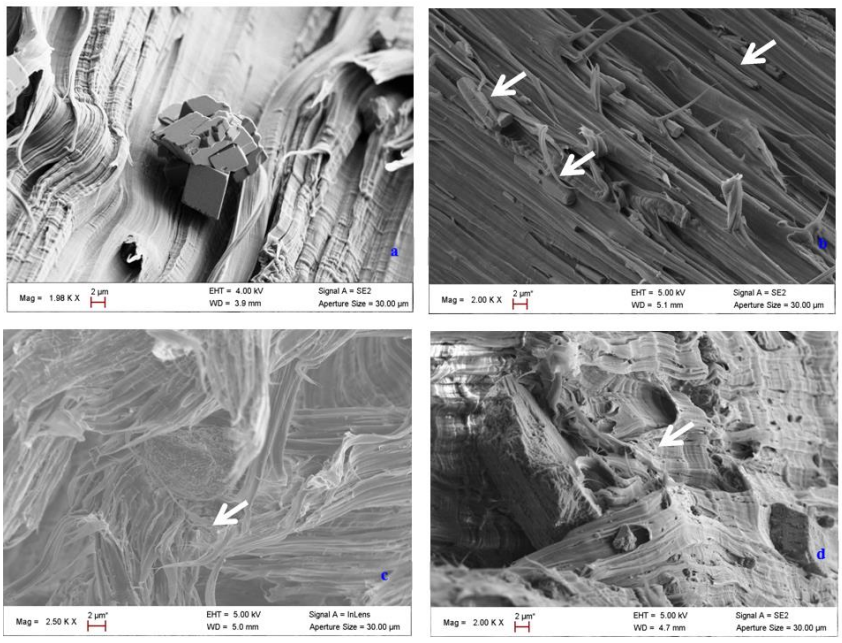

Figure 4. SEM pictured of fractured PE-$CaCO_3$ Tensile Specimens a) PE-calcite b) PE-aragonite c) PE-*C. gigas* d) PE-*C. Fornicata*

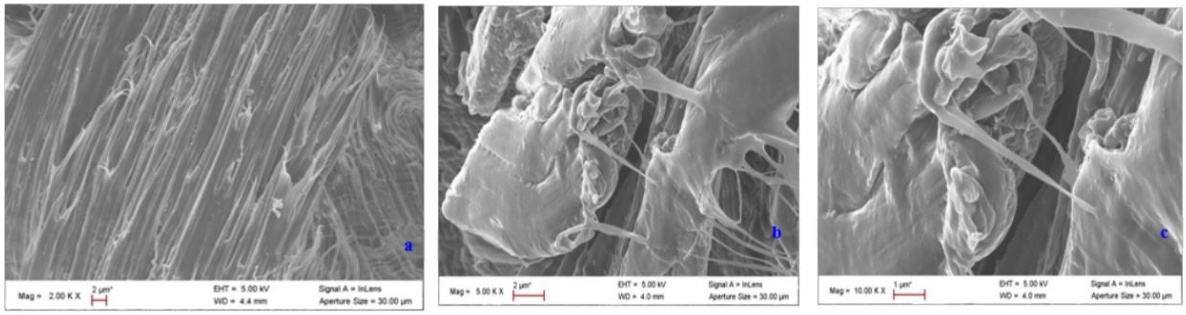

Figure 5. SEM pictures of PE-*C. Fornicata* coated with SA.

Table 1. The shear modulus, young modulus and yield stress of the composite materials

	Filler content (wt%)	Matrix Crystallinity (%)	G* (MPa)	s_y (MPa) (±0,5 MPa)	e_r (%) (±80 %)
PE	0	52	2,8	16	1100
PE-Calcite	9,6	48	3,2	16	720
PE-Calcite -SA	7,7	48	3,1	15	720
PE-Aragonite	10,3	51	3,45	15	910
PE-Aragonite -SA	9,3	53	2,6	16	930
PE-C. Fornicata	8,6	49	2,8	16	670
PE-C. Fornicata -SA	9,5	49	3	15	740
PE-C. Gigas	6,5	52	2,8	16	730
PE-C. Gigas -SA	9,3	50	3,2	15	830
PE-P. Maximus	10,8	47	3	16	680
PE-P. Maximus -SA	9,7	50	3,2	16	760

4. Conclusions

In this study, shell structures of *Crepidula fornicata*, *Crassostrea gigas* and *Pecten maximus* have been characterized by SEM and XRD and their potential use as polymer fillers investigated.

Lamellar and columnar shell microstructures were observed in *Pecten maximus* and *Crepidula fornicata* via scanning electron microscopy. Lamellar laths are observed in the Scallop and in the *Crepidula* species while *Crassostrea gigas* structure exhibits foliated, lamellar, columnar and chalky microstructural morphologies, very different from the microstructures of the two other species.

When these biogenic sources were incorporated in a polymer matrix after grinding, they gave rise to similar impacts on the polymer structural and mechanical properties as the synthetic mineral calcium carbonates when aggregation is limited by using a stearic acid treatment. Even if a significant effect of the presence of organic molecules in these biogenic fillers has been detected, no detrimental effects have been observed. Biogenic calcium carbonate sources, which are usually considered as wastes from several industries can therefore be used as fillers in the compounding industry and lead to composite materials with properties equivalent to classically filled polymers.

Funding

This research received no external funding.

Conflicts of Interest

The authors declare no conflict of interest.

Acknowledgement

This study was performed in "Laboratoire de Chimie Moléculaire et Thio-organique" (CNRS UMR 6507) and "Laboratoire de CRIstallographie et Science des MATériaux » (CNRS UMR 6508). Authors wish to thank TUBITAK 2219 post-doc research fellowship for support and also gratefully thank Clément Paul forprecious discussions.

References

1. Dauphin, Y.; Luquet, G.; Salome, M.; Bellot–Gurlet, L.; Cuif, J.P. Structure and composition of Unio pictorum shell: arguments for the diversity of the nacroprismatic arrangement in molluscs. *J. Microsc.* **2018** *Volume 270, Issue 2*, pp. 156-169. https://doi.org/10.1111/jmi.12669

2. Chateigner, D.; Ouhenia, S.; Krauss, C.; Belkhir, M.; Morales, M. Structural distortion of biogenic aragonite in strongly textured mollusk shell layers. *Nucl. Instrum. Methods Phys. Res. B* **2010**, *Volume 268, Issues 3-4*, pp. 341-345. https://doi.org/10.1016/j.nimb.2009.07.007

3. Chateigner, D.; Ouhenia, S.; Krauss, C.; Hedegaard, C.; Gil, O.; Morales, M.; Lutterotti, L.; Rousseau, M.; Lopez, E. Voyaging around nacre with the X-ray shuttle: From bio-mineralisation to prosthetics via mollusk phylogeny. *Mat. Sci. Eng. A-Struct.* **2010**, *Volume 528, Issue 1*, pp. 37-51. https://doi.org/10.1016/j.msea.2010.07.032

4. Yang, W.; Zhang, G.P.; Zhu, X.F.; Li, X.W.; Meyers, M.A. Structure and mechanical properties of *Saxidomus purpuratus* biological shells. *J. Mech. Behav. Biomed. Mater.* **2011**, *Volume 4, Issue 7*, pp. 1514-1530. https://doi.org/10.1016/j.jmbbm.2011.05.021

5. Neves, N.M.; Mano, J.F. Structure/Mechanical behaviour relationships in crossed-lamellar sea shells. *Mater. Sci. Eng. C* **2005** *Volume 25, Issue 2*, pp. 113-118

6. Lee, S.W.; Kim, G.H.; Choi, C.S. Characteristic crystal orientation of folia in oyster shell, *Crassostrea gigas*. *Mater. Sci. Eng. C* **2008**, *Volume 28, Issue 2*, pp. 258-263

7. Pokroy, B.; Fitch, A.N.; Zolotoyabko, E. The Microstructure of Biogenic Calcite: A View by High-Resolution Synchrotron Powder Diffraction. *Adv. Mater.* **2006,** *Volume 18, Issue 18*, pp. 2363-2368. https://doi.org/10.1002/adma.200600714

8. Kunitake, M.E.; Mangano, L.M.; Peloquin, J.M.; Baker, S.P.; Stroff, L.A. Evaluation of strengthening mechanisms in calcite single crystals from mollusc shells. *Acta Biomater.* **2013** *Volume 9, Issue 2*, pp. 5353-5359

9. Lee, S.W.; Jang, Y.N.; Ryu, K.W.; Chae, S.C.; Lee, Y.H.; Jeon C.W. Mechanical characteristics and morphological effect of complex crossed structure in biomaterials: fracture mechanics and microstructure of chalky layer in oyster shell. *Micron* **2011** *Volume 42, Issue 1,* 60-70

10. Marin, F.; Luquet, G. Molluscan shell proteins. C. R. *Palevol.* **2004**, *Volume 3, Issues 6-7*, pp. 469-492. https://doi.org/10.1016/j.crpv.2004.07.009

11. Takeuchi, T.; Sarashina, I.; Iijima, M.; Endo, K. In vitro regulation of $CaCO_3$ crystal polymorphism by the highly acidic molluscan shell protein Aspein. *FEBS Lett.* **2008**, *Volume 582, Issue 5*, pp. 591-596. https://doi.org/10.1016/j.febslet.2008.01.026

12. Morris, J.P.; Backeljau, T.; Chapelle, G. Shells from aquaculture: a valuable biomaterial, not a nuisance waste product. *Rev. Aquacult.* **2019**, *Volume 11, Issue 1*, pp. 42-57. https://doi.org/10.1111/raq.12225

13. Fombuena, V.; Bernardi, L.; Fenollar, O.; Boronat, T.; Balart, R. Characterization of green composites from biobased epoxy matrices and bio-fillers derived from seashell wastes. *Mater. Design.* **2014**, *Volume 57,* 168-174. https://doi.org/10.1016/j.matdes.2013.12.032

14. Samant, S.; Naik, M.M.; Vaingankar, D.C.; Mujawar, S.Y.; Parab, P.; Meena, S.N. Chapter 1: Biodegradation of fish waste by seaweed associated bacteria and application of seafood waste for ethanol production. *Advances in Biological Science Research, A Practical Approach* **2019**, Academic Press, 149-158

15. Sharma, S.K.; Pujari, P.K. Role of free volume characteristics of polymer matrix in bulk physical properties of polymer nanocomposites: A review of positron annihilation lifetime studies. *Prog. Polym. Sci.* **2017**, *Volume 75*, pp. 31-47

16. Lazzeri, A.; Zebarjad, S.M.; Pracella, M.; Cavalier, K.; Rosa, R. Filler toughening of plastics. Part 1- The effect of surface interactions on physico-mechanical properties and rheological behavior of ultrafine $CaCO_3$/HDPE nanocomposites. *Polymer* **2005**, *Volume 46, Issue 3*, pp. 827- 844

17. Gai, G.S.; Yang, Y.F.; Fan, S.M.; Cai, Z.F. Preparation and properties of composite mineral powders. *Powder Technol.* **2005**, *Volume 153, Issue 3*, pp. 153-158

18. González, J.; Albano, C.; Candal, M.V.; Ichazo, M; Hernández, M.; Mayz, A.A.; Martínez, A. Characterization of composites based in polyolefins and seashells. *Rev. Fac. Ing. Univ. Centr. Ven.* **2006**, *Volume 21, Issue 3,* pp. 89-104

19. Zare, Y.; Rhee, K.Y. Modeling the roles of carbon nanotubes and interphase dimensions in the conductivity of nanocomposites. *Appl. Clay Sci.* **2017,** *Volume 150, Issue 15*, pp. 102562. https://doi.org/10.1016/j.rinp.2019.102562

20. Lucas, A.; Gaudé, J.; Carel, C.; Michel, J.–F.; Cathelineau, G. A synthetic aragonite-based ceramic as a bone graft substitute and substrate for antibiotics. *Int. J. Inorg. Mater.* **2001**, Volume 3, Issue 1, 87-94

21. Chakrabarty, D.; Mahapatra, S. Aragonite crystals with unconventional morphologies. *J. Mater. Chem.* **1999,** *Volume 9, Issue 11,* pp. 2953-2957. https://doi.org/10.1039/a905407c

22. Dobircau, L.; Delpouve, N.; Herbinet, R.; Domenek, S.; Le Pluart, L.; Delbreilh, L.; Ducruet, V.; Dargent, E. Molecular mobility and physical ageing of plasticized poly(lactide). *Polym. Eng. Sci.* **2015**, *Volume 55, Issue 4*, pp. 858-865. https://doi.org/10.1002/pen.23952

23. White, J.L.; Kim, E.K. (Eds.) "Twin Screw Extrusion: Technology and Principles", Hanser Publishers, New York, **1991**

24. Carter, J.G.; Clark, G.R. Classification and phylogenetic significance of molluscan shell microstructure. In: Molluscs, Notes for a Short Course. University of Tennessee, Department of Geological Sciences, Studies in Geology Publishers, Volume 13; Bottjer, D.J.; Hickman, C.S.; Ward, P.D.; Broadhead, T.W. (Eds.) **1985**, pp. 50-71

25. Chateigner, D.; Hedegaard, C.; Wenk, H.R. Mollusc shell microstructures and crystallographic textures. *J. Struct. Geol.* **2000**, *Volume 22, Issue 11*, pp. 1723-1735

26. Chateigner, D. (Ed.), "Combined Analysis", Wiley-ISTE Publishers, **2010**.

27. Rietveld, H.M. A profile refinement method for nuclear and magnetic structures. *J. Appl. Cryst.* **1969**, *Volume 2,* pp. 65-71. https://doi.org/10.1107/S0021889869006558

28. Lutterotti, L.; Bortolotti, M. Object oriented programming and fast computation techniques in Maud, a program for powder diffraction analysis written in java. *IUCr: Com. Powd. Diff. Newsletter* **2003**, *Volume 1*, pp. 43-50

29. Ouhenia, S.; Chateigner, D.; Belkhir, M.A.; Guilmeau, E.; Krauss, C. Synthesis of Calcium Carbonate Polymorphs in the Presence of Polyacrylic Acid. *J. Cryst. Growth.* **2008**, *Volume 310, Issue 11*, pp. 2832-2841

30. Grazulis, S.; Chateigner, D.; Downs, R.T.; Yokochi, A.F.T.; Quiros, M.; Lutterotti, L.; Manakova, E.; Butkus, J.; Moeck, P.; Le Bail, A. Crystallography Open Database- an open- Access collection of crystal structures. *J. Appl. Cryst.* **2009**, *Volume 42, Issue 4*, pp. 726-729

31. Caspi, E.N.; Pokroy, B.; Lee, P.L.; Quintana, J.P.; Zolotoyabko, E. On the structure of aragonite. *Acta Cryst. B* **2005**, *Volume 61,* pp. 129-132

32. Popa N.C. The (hkl) dependence of diffraction-line broadening caused by strain and size for all Laue groups in Rietveld refinement, *J. Appl. Cryst.* 1998, *Volume 31*, 176-180

33. Esteban-Delgado, F.J.; Harper, E.M.; Checa, A.G.; Rodriguez-Navarro, A.B. Origin and expansion of foliated microstructure in pteriomorph bivalves. *Biol. Bull.* **2008,** *Volume 214, Issue 2*, pp. 153-165. https://doi.org/10.2307/25066672

34. MacDonald, J.; Freer, A.; Cusack, M. Alignment of Crystalographic c-Axis throughout the Four Distinct Microstructural Layers of the Oyster *Crassostrea gigas*. *Cryst. Growth Des.* **2010**, *Volume 10, Issue 3*, pp. 1243-1246. https://doi.org/10.1021/cg901263p

35. Checa, G.; Esteban-Delgado, F.J.; Ramírez-Rico, J. Crystallographic reorganization of the calcitic prismatic layers of oysters *J. Struct. Biol.* **2009**, *Volume 167, Issue 3,* 261-270

36. Taylor, P.D.; Weedon, M.J. Skeletal ultrastructure and phylogeny of cyclostome bryozoans. *Zool. J. Linnean Soc.* **2000**, *Volume 128, Issue 4*, pp. 337-399. https://doi.org/10.1111/j.1096-3642.2000.tb01521.x

37. England, J.; Cusack, M.; Dalbeck, P.; Perez-Huerta, A. Comparison of the Crystallographic Structure of Semi Nacre and Nacre by Electron Backscatter Diffraction. *Cryst. Growth Des.* **2007**, *Volume 7, Issue 2*, pp. 307-310. https://doi.org/10.1021/cg060374p

38. Chateigner, D.; Morales, M.; Harper, E.M. QTA of prismatic calcite layers of some bivalves, a link to trichite ancestrals. *Mater. Sci. Forum* **2002**, *Volume 408-412*, 1687-1692

39. Misra, R.D.K; Nerikar, P.; Bertrand, K.; Murphy, D. Some aspects of surface deformation and fracture of 5-

20% calcium carbonate-reinforced polyethylene composites. *Mat. Sci. Eng. A* **2004**, *Volume 384, Issue 1-2,* 284-298

40. Shi, X.; Rosa, R.; Lazzeri, A. On the coating of precipitated calcium carbonate with stearic acid in aqueous medium. *Langmuir* **2010**, *Volume 26, Issue 11*, pp. 8474-8482. https://doi.org/10.1021/la904914h

41. Kiss, A.; Fekete, E.; Pukanszky, B. Aggregation of $CaCO_3$ particles in PP composites: effect of surface coating. *Compos. Sci. Technol.* **2007,** *Volume 67, Issue 7-8*, pp. 1574-1583

42. Sahebian, S.; Zebarjad, S.M.; Sajjadi, S.A.; Sherafat, Z.; Lazzeri, A. Effect of both uncoated and coated calcium carbonate on fracture toughness of HDPE/$CaCO_3$ nanocomposites. *J. Appl. Polym. Sci.* **2007**, *Volume 104, Issue 6*, pp. 3688-3694. https://doi.org/10.1002/app.25644

43. Kutz, M. (Ed.) "Handbook of environmental degradation of Materials", **2012** William Andrew Publisher, UK

Supplementary Materials

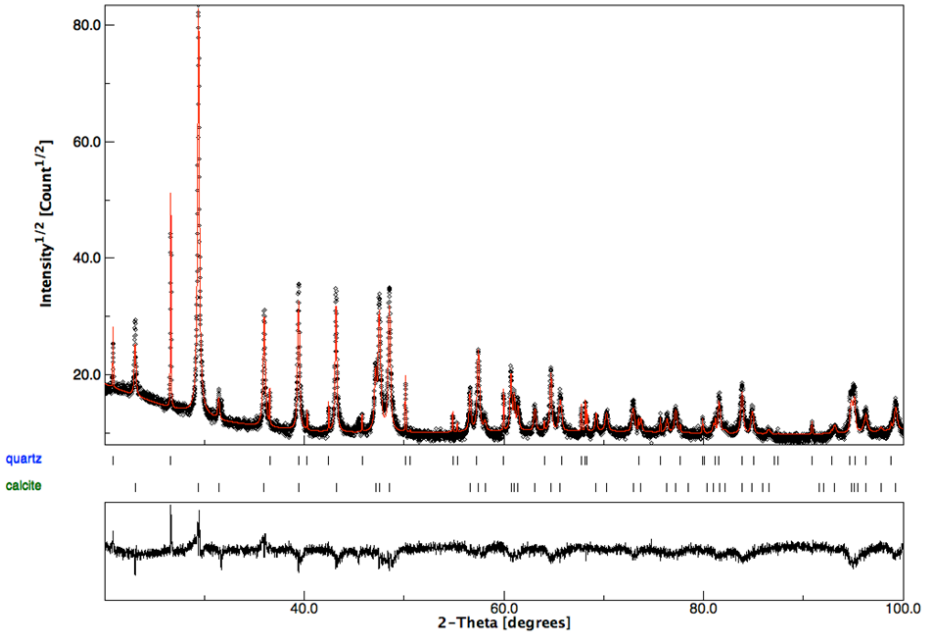

Supplementary Figure 1. XRD pattern and corresponding Combined Analysis fit of the ground *Pecten maximus* layers of Figure 1. CoFe peaks come from the sample holder. Goodness of Fit is 1.68. Residual aragonite is seen as very small peaks. Inset is the refined anisotropic mean shape of crystallites.

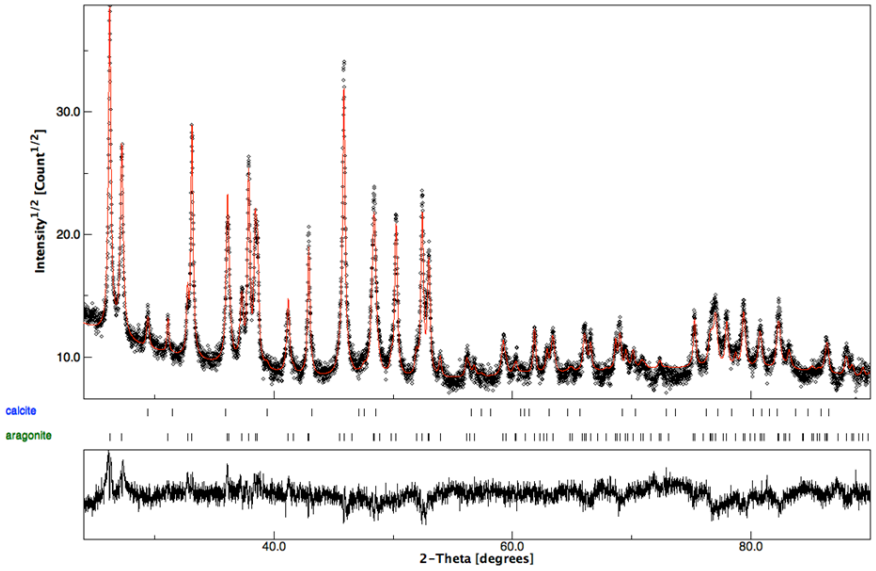

Supplementary Figure 2. XRD pattern and corresponding Combined Analysis fit of the ground *Crepidula fornicata* layers of Figure 3. Goodness of Fit is 1.33. Insets are the refined anisotropic mean shape of crystallites and SEM image of the powder.

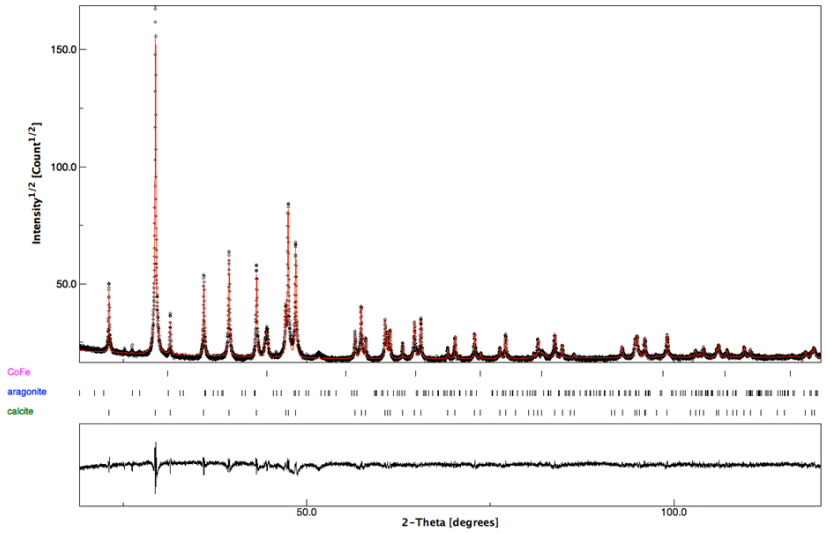

Supplementary Figure 3. XRD pattern and corresponding Combined Analysis fit of the ground *Crassostrea gigas* layers of Figure 5. Goodness of Fit is 1.66. Insets are the refined anisotropic mean shape of crystallites and SEM image of the powders. Residual quartz comes from incorporated sand in the outer part of the shell

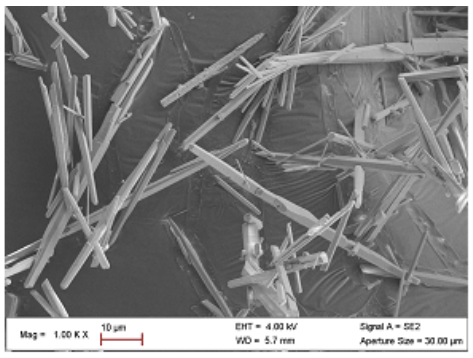

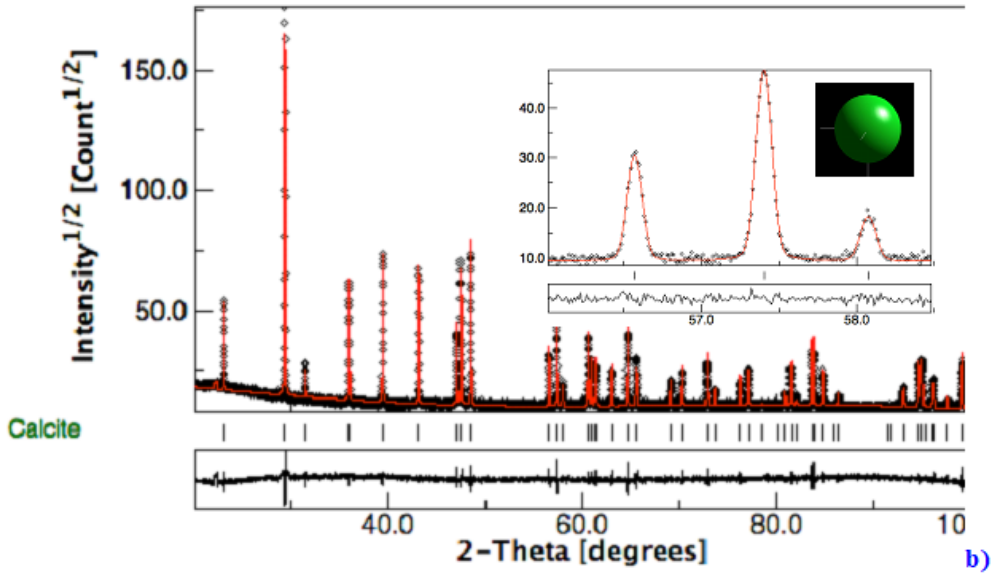

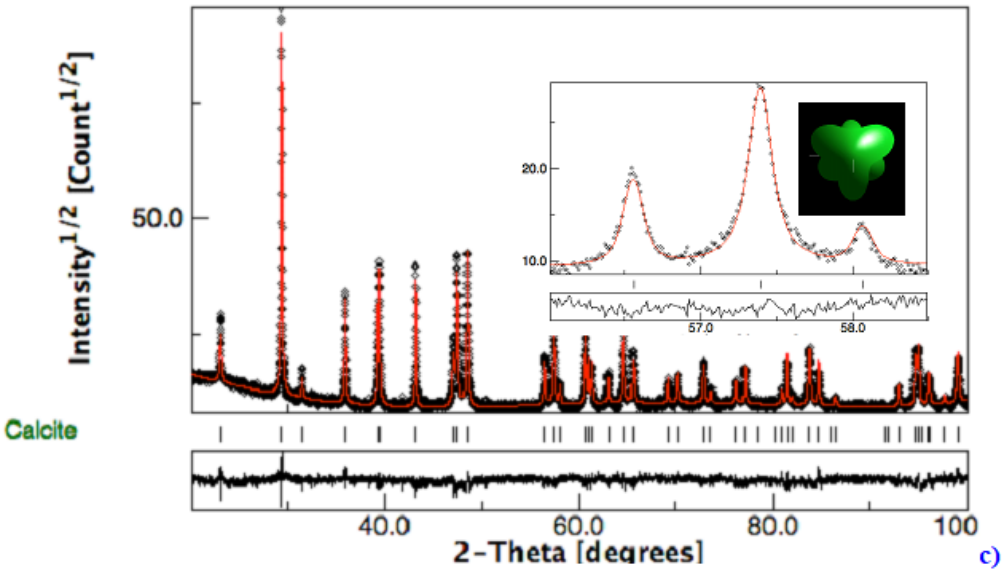

Supplementary Figure 4. a) Synthesized aragonite powder and **b)** XRD pattern and fit of Commercial calcite as received (GoF = 2.2) **c)** XRD pattern and fit of the ground commercial calcite (GoF = 1.4). Insets in b) and c) are zooms of the calcite diffraction line broadening increase due to grinding in the 2θ = 56°-58.5° range, with their respective mean crystallite shapes

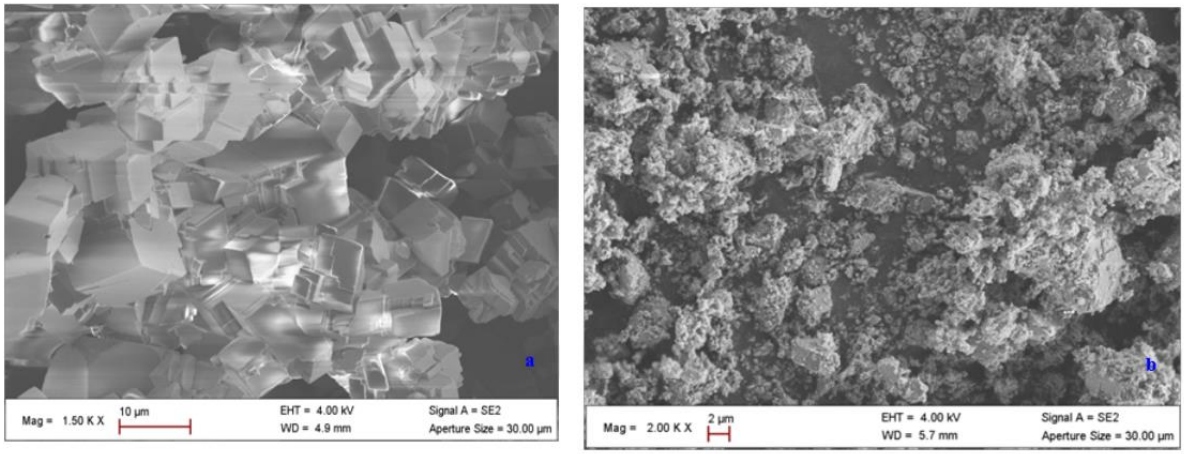

Supplementary Figure 5. SEM images of commercial calcite samples a) before and b) after grinding

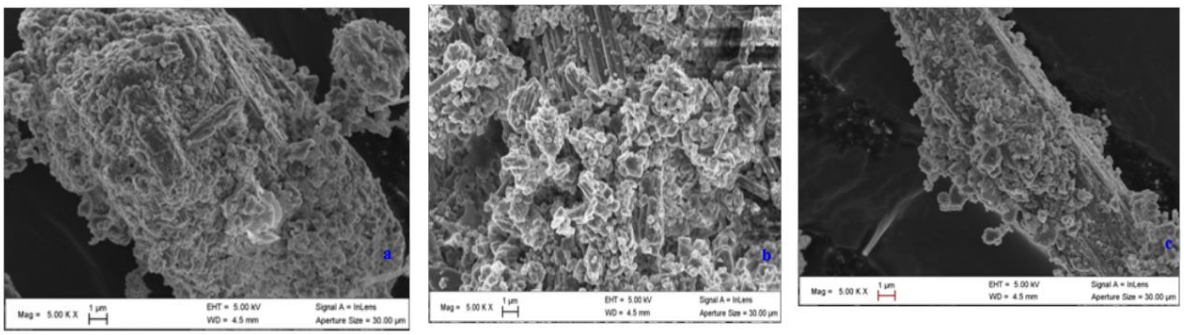

Supplementary Figure 6. SEM pictures of SA coated a) *C. Fornicata b) P. Maximus and c) C. Gigas* powders